

## RESEARCH ARTICLE

# Beyond muscles: role of intramuscular connective tissue elasticity and passive stiffness in octopus arm muscle function

Alessio Di Clemente<sup>1,2,\*</sup>, Federica Maiole<sup>1,2,\*</sup>, Irene Borgia<sup>1</sup> and Letizia Zullo<sup>2,3,‡</sup>

## ABSTRACT

The octopus arm is a ‘one of a kind’ muscular hydrostat, as demonstrated by its high maneuverability and complexity of motions. It is composed of a complex array of muscles and intramuscular connective tissue, allowing force and shape production. In this study, we investigated the organization of the intramuscular elastic fibers in two main muscles composing the arm bulk: the longitudinal (L) and the transverse (T) muscles. We assessed their contribution to the muscles’ passive elasticity and stiffness and inferred their possible roles in limb deformation. First, we performed confocal imaging of whole-arm samples and provided evidence of a muscle-specific organization of elastic fibers (more chaotic and less coiled in T than in L). We next showed that in an arm at rest, L muscles are maintained under 20% compression and T muscles under 30% stretching. Hence, tensional stresses are inherently present in the arm and affect the strain of elastic fibers. Because connective tissue in muscles is used to transmit stress and store elastic energy, we investigated the contribution of elastic fibers to passive forces using step-stretch and sinusoidal length-change protocols. We observed a higher viscoelasticity of L and a higher stiffness of T muscles, in line with their elastic fiber configurations. This suggests that L might be involved in energy storage and damping, whereas T is involved in posture maintenance and resistance to deformation. The elastic fiber configuration thus supports the specific role of muscles during movement and may contribute to the mechanics, energetics and control of arm motion.

**KEY WORDS:** Cephalopod, Muscular hydrostat, Motor control, Muscle damping, Muscle stiffness, Muscle elasticity

## INTRODUCTION

Hydrostatic limbs are constant-volume structures made up of densely packed, three-dimensional arrays of muscle and connective tissue fibers. Because of the broad changes in body shape they can undergo, any deformation also induces a redistribution of hydrostatic pressure within the limb. To compensate for variation in pressure, these structures often manifest strain gradients across the muscular body that can be modified during motion (Kurth et al., 2014).

Intramuscular connective tissue represents a fundamental component of hydrostatic muscles, as it provides a means of

transmitting elastic energy and imposing stiffness on an unrestrained soft structure lacking internal or external rigid components, thus controlling and limiting shape changes (Kier, 2012).

The octopus arm is a ‘one of a kind’ muscular hydrostat as a result of its high maneuverability and the complexity of motion performed. Given that, it might represent an ideal model for studying the role of tensional stress during hydrostatic limb deformations, such as elongation, compression and bending. The octopus arm is a compact structure with no fluid or air-filled cavities. It is composed almost entirely of a three-dimensional array of muscle fibers, a central axial nerve cord carrying information to and from the central brain (Graziadei, 1971; Zullo et al., 2019, 2011), and two lines of suckers. The longitudinal (L) muscles make up the main outer muscle layer of the arm bulk, with muscle fibers oriented parallel to the arm longitudinal axis. They enclose the transverse (T) muscle mass, with muscle fibers oriented in multiple planes perpendicular to the longitudinal axis of the arm (Fig. S1).

The arm muscles are embedded within a dense connective matrix of connective tissue (Fossati et al., 2011; Kier and Stella, 2007), organized in a rich network of intramuscular collagen fibers (Kurth et al., 2014) and a dispersed matrix of extracellular components. Because of its mechanical properties, collagen has both intrinsic limited extensibility and inherent stiffness, but it can reach a certain degree of elasticity through the coiling of collagen fibers. The presence and organization of coiled elastic components has been widely described in another type of muscular hydrostat, squid mantle muscles, and they have been shown to play an important role in controlling deformation (Kier and Stella, 2007; Thompson and Kier, 2001).

The arrangement of elastic components in the octopus arm is an under-investigated topic, with no attempt to show its functional role during motion. It is important to consider that elastic elements are also relevant to muscle active contraction, as they can function like locomotor springs, alternatively storing and releasing elastic energy as animals move. They can also be employed as elements to resist shortening during active contraction and produce stiffening of the limb. In the octopus arm, stiffening can be used for a variety of functions, such as counteracting longitudinal compression, bending at precise locations and producing semi-rigid structures.

In this work, we aimed at investigating the arrangement and role of connective tissue in octopus arm muscle function. We performed a detailed analysis of the *Octopus vulgaris* arm intramuscular connective tissue organization and assessed the effect of tensional stresses on the elastic behavior and stiffness of muscles. In particular, we asked whether, similar to other muscular hydrostats, tensional stress is able to generate strain that affects the configuration of the elastic collagen fibers. If so, an arm would be able to rely during motion on readily releasable energy stored within its elastic components. In addition, being completely passive,

<sup>1</sup>University of Genova, Viale Benedetto XV, 3, 16132 Genova, Italy. <sup>2</sup>Center for Micro-BioRobotics & Center for Synaptic Neuroscience and Technology (NSYN), Istituto Italiano di Tecnologia, Largo Rosanna Benzi 10, 16132 Genova, Italy.

<sup>3</sup>IRCSS, Ospedale Policlinico San Martino, Largo Rosanna Benzi 10, 16132 Genova, Italy.

\*These authors contributed equally to this work

‡Author for correspondence (letizia.zullo@iit.it)

 L.Z., 0000-0003-0503-6312

elastic elements may represent an important means of reducing the overall energetic and computational cost of the active arm ‘reconfiguration’.

## MATERIALS AND METHODS

### Animal treatment

A total of 21 *Octopus vulgaris* Cuvier 1797 specimens were used for this study. Animals of both sexes (mass range, 200–300 g) were collected from October to May from local anglers on the Ligurian coast of Italy. All our research conformed to the ethical principles of the three Rs (replacement, reduction and refinement) and of minimizing animal suffering, following Directive 2010/63/EU (Italian D. Lgs. no. 26/2014) and the guidelines from Fiorito et al. (2014, 2015). All experimental procedures were approved by the Institutional Board and the Italian Ministry of Health (authorization no. 465/2017-PR).

After the capture, animals were placed in 80×50×45 cm aquarium tanks filled with artificial seawater (Tropic Marin Pro Reef) and enriched with sand substrate and clay pot dens. The temperature was maintained constant at 17°C, corresponding to the average temperature at the collection site, and was continuously circulated through a biological filter system. Oxygenation was ensured by a dedicated aeration system, and all relevant water chemical/physical parameters were checked daily. The animals were left to adapt for at least 5 days before the experiments. They were inspected daily and fed shrimp 3 times a week.

Before the experiments, the animals were anesthetized in 3.5% MgCl<sub>2</sub> seawater. A short whole arm sample was cut from the medial portion of one arm (L2, L3 or R2) and kept in oxygenated seawater at 16°C for both histology and biomechanics procedures.

### Histology

Arm samples from six different specimens were fixed overnight in 4% paraformaldehyde (PFA) in artificial seawater (ASW: NaCl 460 mmol l<sup>-1</sup>, KCl 10 mmol l<sup>-1</sup>, MgCl<sub>2</sub> 55 mmol l<sup>-1</sup>, CaCl<sub>2</sub> 11 mmol l<sup>-1</sup>, Hepes 10 mmol l<sup>-1</sup>, glucose 10 mmol l<sup>-1</sup>; pH 7.6), cryopreserved in 30% sucrose overnight, embedded in O.C.T. compound (Electron Microscopy Sciences), and sectioned to obtain 20 μm slices with a cryostat microtome (MC5050 Cryostat Microtome). Samples were sectioned following a longitudinal or transverse plane to analyze, respectively, the organization of the L or T muscle bundles.

To visualize the tissue collagen content, slices were stained with a Picrosirius Red (PSR) kit (04-121873, Bio Optica) following the manufacturer’s protocol and mounted with coverslips using DPX mountant.

Sequential images of longitudinal and transverse arm sections were acquired using a confocal laser scanning microscope (Leica SP8). PSR-stained elastic fibers show fluorescence in the red spectra, thus allowing a confocal reconstruction of their structure through the z planes (Vogel et al., 2015). PSR-stained sections were excited at 560 nm, and the emitted light was collected at 570–700 nm.

Images were then examined using ImageJ software to assess the collagen fiber structure and organization. In particular, the elastic fibers were described using two indexes: the waviness index (WI) quantifying their coiling rate, as described in Kurth et al. (2014), and the chaos index (CI) describing their spatial organization.

WI is a dimensionless index, defined as the ratio between the total length of a fiber and its end-to-end straight-line distance (Kurth et al., 2014), thus representing the fiber’s degree of coiling. When WI=1, the fiber is in an uncoiled state, while WI >1 indicates fiber coiling (Fig. 1A).

WI was analyzed in small whole-arm samples (4–8 mm in length) at rest and when stretched at various degrees of their length (0%, 10% and 30%) following this procedure: (1) fix the sample at one end with aluminium staples on a plastic support, (2) measure the sample longitudinal resting length with a caliper under a dissection microscope, (3) gently pull the sample with forceps in a longitudinal direction till reaching the desired percentage elongation, (4) block the sample in this configuration by stapling the other end to the plastic support, (5) dip it in a bath containing PFA and fix it overnight. Twelve samples (three for each condition) from three different animals were employed for each muscle type. Application of a longitudinal stretch to the arm induces the L muscles to elongate by an amount equal to the given elongation and T muscle (oriented perpendicularly to the force applied) to shorten by an amount proportional to the square root of the imposed length change and calculated as follows:

$$\frac{r_f}{r_i} = \sqrt{\frac{l_i}{l_f}} \quad (1)$$

where  $r_i$  and  $r_f$  are the initial and final radius, respectively; and  $l_i$  and  $l_f$  are the initial and final length of the arm segment, respectively.

CI, defined as the angle between the elastic fiber axis and the main muscle force axis (Fig. 1B), was calculated in the arm samples at rest. Three samples from three different animals were used for each muscle type. CI ranges were between 0 and ±90 deg, where 0 deg indicates a fiber parallel and ±90 deg indicates a fiber perpendicular to the main muscle force axis (Fig. 1C).

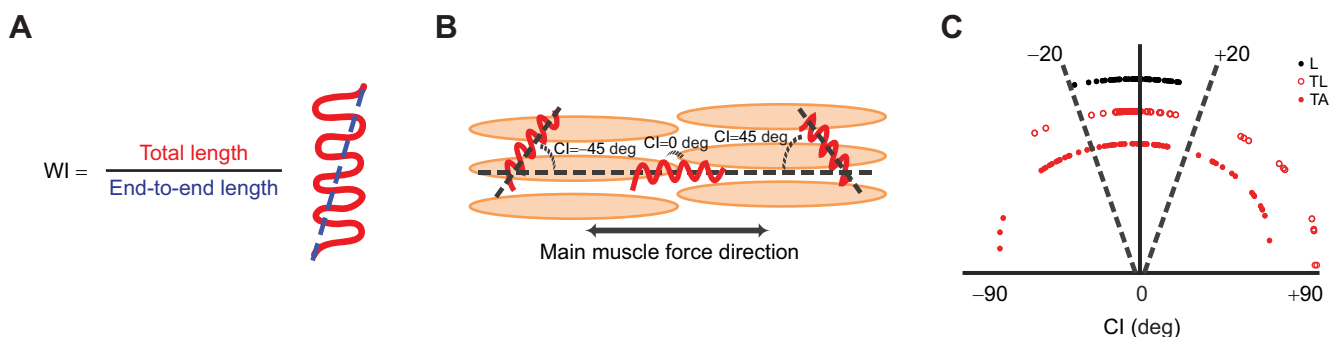


**Fig. 1. Elastic fiber characterization.** (A) The waviness index (WI) was calculated as the ratio between the total length of the fiber and its end-to-end length (dotted line). (B) The chaos index (CI) was calculated as a measure of the angle between the main muscle force direction (double-headed arrow) and the elastic fiber orientation (dashed lines). (C) Exemplary distribution of elastic fiber orientation in longitudinal (L), transverse lateral (TL) and transverse aboral (TA) muscles.

### Ex vivo muscle measurements

Twenty-one whole-arm samples (5–10 mm in length) from four different animals were hand cut with a scalpel from the middle portion of 11 arms. Skin and suckers were rapidly removed, and L or T aboral proximo-distal (P-D), latero-lateral (L-L) and oral-aboral (O-A) dimensions were measured with a caliper under a dissection microscope in the whole-arm configuration (Fig. 2A). Each measurement was taken from two independent experimenters to account for individual variability. In detail, for the L aboral muscles, P-D was measured as the end-to-end distance of the whole-arm segment, O-A as its O-A maximum dimension (with no derma included), and L-L as its side-to-side maximum width (see Fig. 2A). For the T aboral muscles, P-D was considered as the end-to-end distance of the whole-arm segment, O-A as its O-A minor dimension, and L-L as its side-to-side minimum width (see Fig. 2A).

Next, the entire L or T aboral muscle strips were removed from the whole-arm segment. To dissect the L aboral muscles, the dermal surface of the arm was removed. Two longitudinal incisions were made at the L lateral edges, and a third longitudinal incision was made at the boundary between the L aboral and T aboral muscles. To dissect the T aboral muscles, two longitudinal incisions were made at the edge between the T aboral and L lateral muscles, and two incisions were made at the upper and lower T aboral edges.

The dimensions of the dissected L and T muscle strips were then measured using a caliper under a dissection microscope. The length of the dissected muscle was considered as the muscle resting length ( $L_R$ ) and used as a reference to calculate T and L muscle length inside the arm in the whole-arm configuration ( $L_{in}$ ), further expressed as a percentage of  $L_R$  (Fig. 2B).

### Muscle biomechanics

#### Muscle preparation

A small strip of muscles (4–8 mm) was dissected by hand from the aboral portion of the L or T arm muscles (Fig. S1). For simplicity,

we hereafter refer to them as T (transverse) and L (longitudinal) muscles. Thirty-two samples (15 T and 17 L) from 11 different specimens were employed. To dissect the L muscles, the epidermis and dermal connective tissue were first removed with the circumferential and oblique muscle layers. Then, a strip of the L muscles was cut from the arm, following a P-D axis. We thus obtained a bundle of L muscles containing thin longitudinal sheets of transverse fibers (the so-called trabeculae; Graziadei, 1971) located between bundles of L muscle and oriented perpendicular to the longitudinal axis (Kier, 2016; Kier and Stella, 2007). To dissect the T muscles, a thin transverse arm slice (2–4 mm thick) was cut, and a rectangular strip of only T muscles was removed from its central portion following the L-L axis. Given the intrinsic organization of the transverse muscle fibers, the T muscle bundle we obtained comprised fibers oriented in multiple planes perpendicular to the longitudinal axis. At the end of the experimental session, the height ( $h$ ) and width ( $w$ ) of T and L muscle strips were measured at rest with an electronic caliper under a dissection microscope.

The T and L muscle strip samples were assumed to hold a parallelepiped shape, and their cross-sectional area (CSA) was calculated according to Eqn 2:

$$CSA_{par} = h \cdot w. \quad (2)$$

Muscle strips were mounted on the recording chamber of a Dual Mode Lever Arm System (ASI 300C-LR, Aurora Scientific Instruments). Samples were attached to a micrometer block on one end and to a lever arm on the other using suture threads (silk suture threads 5/0, Ethicon Inc., code: K880H) and tightened with double square knots. The muscle strip was adjusted to allow a small transient passive force to develop; muscle resting length ( $L_R$ ) was determined in this condition by measuring the distance between the knots with an electronic caliper. The recording chamber was continuously perfused with oxygenated ASW at 16°C using a

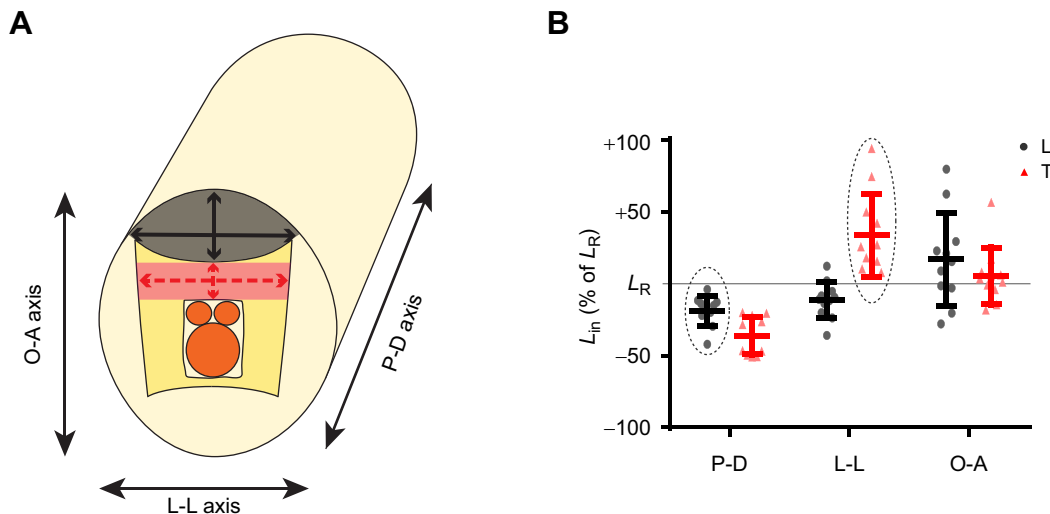


**Fig. 2. Muscle length inside the arm.** (A) Schematic representation of T (red shading) and L (gray shading) muscle sample dissection and methodology employed for *ex vivo* measurements. Oral-aboral (O-A), latero-lateral (L-L) and proximo-distal (P-D) axes are indicated. In the L aboral muscles, P-D was measured as the end-to-end distance of the whole-arm segment, O-A as its O-A maximum dimension (with no derma included) and L-L as its side-to-side maximum width (black arrows). In the TA muscles, P-D was considered as the end-to-end distance of the whole-arm segment, O-A as its O-A minor dimension and L-L as its side-to-side minimum width (red dashed arrows). (B) Length of T ( $n=10$ ) and L ( $n=11$ ) muscles inside the arm ( $L_{in}$ ).  $L_{in}$  is expressed as a percentage of the resting length ( $L_R$ ) of the muscle once dissected from the arm. Measurements were taken in three axes: P-D, L-L and O-A. Symbols are individual data points and bars show means  $\pm$  s.d. Dashed ellipses highlight the axis along which T and L muscle fibers are oriented (i.e. their main force axis). Note that L muscles are compressed along their main force axis, with a length inside the arm of  $-20\%$  of their  $L_R$  outside the arm. Conversely, T muscles are stretched, with a length inside the arm of  $+30\%$  of their  $L_R$  outside the arm.

peristaltic pump (SJ-1220, Atto Co.). Particular attention was paid to making sure that perfusion flux did not induce noise in the force recordings. The recordings were digitized and analyzed using a LabVIEW-based data acquisition and analysis system (ASI 604A and 605A, Aurora Scientific Instruments). Data were acquired at a 10 kHz sampling frequency and filtered with a low-pass filter at 3.3 kHz.

### Stress–strain relationship

Stiffness was tested using a step-stretch, stress–strain protocol. Mechanical strain ( $\epsilon$ ) ranging from 1% to 60% of  $L_R$  was sequentially applied to the dissected muscle strips with 5% incremental steps. Each strain step was maintained for 10 s, and the resulting force–time trace was recorded and analyzed offline.

The tissue response to mechanical strain is characterized by an early peak force followed by an exponential decline and a late steady-state force. According to the Hill model (Hill, 1938), passive forces in skeletal muscles can be described by the interplay between two elastic components: one organized in series (SE) to the contractile element and the other organized in parallel (PE). Following this model, SE characterizes the early peak force ( $F_{SE}$ ) while PE characterizes the steady-state force, reached upon stabilization ( $F_{PE}$ ).  $F_{SE}$  was measured as the early peak force from the baseline of each step.  $F_{PE}$  was calculated toward the end of each step as the average steady-state force in a 0.5 s interval (Fig. S2). To correct for differences in preparation size, we next calculated the corresponding sample stress ( $\sigma$ ) according to Eqns 3 and 4:

$$\sigma_{SE} = \frac{F_{SE}}{CSA}, \quad (3)$$

$$\sigma_{PE} = \frac{F_{PE}}{CSA}. \quad (4)$$

Young's modulus ( $E$ ) was then calculated according to Eqns 5 and 6 at ranges of strains ( $\epsilon$ ) defined as low (0–15%), medium-low (15–30%), medium-high (30–45%) and high (45–60%):

$$E_{SE} = \frac{\Delta\sigma_{SE}}{\Delta\epsilon}, \quad (5)$$

$$E_{PE} = \frac{\Delta\sigma_{PE}}{\Delta\epsilon}. \quad (6)$$

### Elastic hysteresis

Elastic hysteresis was investigated using a sinusoidal length-change protocol. Starting from their  $L_R$ , samples were subjected to cycles of 2.5 Hz sinusoidal length change with an amplitude equal to 30% of their  $L_R$ . The selection of the experimental parameters was based on relevant classical and more recent literature in which sinusoidal length-change protocols were employed in the context of the work-loop technique (Baxi et al., 2000; Josephson, 1985; Syme and Stevens, 1989). Closed-loop stress–strain profiles were derived from the cycles. Hysteresis percentage ( $H$ ), defined as the ratio between the energy dissipated and the total input energy of the system (Fig. S3), was then calculated as indicated in Eqn 7:

$$H = \frac{E_d}{E_i} \cdot 100, \quad (7)$$

where  $E_d$  is the energy dissipated, calculated as the difference between the area under the ascending and descending phases of the curve in Fig. S3, and  $E_i$  is the total energy input to the system, calculated as the area under the ascending phase of the curve.

### Statistical analysis

Prism 8 software (Graphpad Software Inc.) was used for the statistical analysis. Normality of the datasets was assessed using the D'Agostino and Pearson omnibus normality test. Student's  $t$  or Mann–Whitney tests were used to compare two experimental groups with parametric and non-parametric distributions, respectively. Comparisons among three or more groups were performed using an ordinary one-way ANOVA or Kruskal–Wallis test to compare parametric and non-parametric datasets, respectively. In both cases, the analysis of variance was followed by Dunn's multiple comparisons test. Repeated measures (RM) two-way ANOVA followed by Šidák's multiple comparison was used to analyze stress–strain curves and Young's modulus. Data fitting was performed using the ordinary least squares method.

## RESULTS

### Elastic fiber architecture and organization

We investigated the spatial organization and coiling of elastic fibers embedded in the arm connective matrix by staining whole-arm sections with PSR. PSR-stained fibers appear as bright red helical structures (Fig. 3A–C) against a dark background.

To provide a quantitative measure of their arrangement within the tissue, we employed the two indexes described in Materials and Methods: the chaos index (CI) and the waviness index (WI).

### Chaos index

We first assessed the spatial organization of the elastic fibers in whole-arm samples in the resting state (Fig. 3). The CI in the L aboral (Fig. 3A,C), the T lateral (TL) (Fig. 3B) and T aboral (TA) muscles was analyzed according to their positions in the arm (see Fig. S1). CI significantly differed between the three groups, with elastic fibers in L oriented mainly parallel to the main muscle force direction ( $-20 \text{ deg} < \text{CI} < +20 \text{ deg}$ ) and elastic fibers in T having a more chaotic arrangement and oriented in all directions (see Fig. 1C; TL:  $-30 \text{ deg} < \text{CI} < +90 \text{ deg}$ , TA:  $-90 \text{ deg} < \text{CI} < +90 \text{ deg}$ ; Fig. 3D, Kruskal–Wallis test,  $P < 0.01$ ).

### Waviness index

The degree of coiling of the fibers was analyzed by employing a dimensionless WI (see Materials and Methods). Considering their extremely variable CI, the elastic fibers in TA muscles were further subdivided into parallel ( $\text{TA}_p$ ,  $-20 \text{ deg} < \text{CI} < +20 \text{ deg}$ ) and non-parallel ( $\text{TA}_{np}$ ,  $-20 \text{ deg} > \text{CI} > +20 \text{ deg}$ ) groups (see Fig. 3B). Elastic fibers of the L muscles presented the highest coiling (Fig. 3E, Kruskal–Wallis and Dunn's multiple comparisons test,  $P < 0.001$ ). Small differences were observed among the three subgroups of T muscles, with only TL having a significantly higher WI than  $\text{TA}_p$  (Fig. 3E, Kruskal–Wallis and Dunn's multiple comparisons test,  $P < 0.05$ ). No difference was found between  $\text{TA}_p$  and  $\text{TA}_{np}$ , thus showing a consistency in coiling, irrespective of the fiber orientation within the muscle (Fig. 3E, Kruskal–Wallis and Dunn's multiple comparisons test,  $P > 0.05$ ).

It has been reported that muscles of hydrostatic organs can have differences in strain rate in relation to their function and position within the organ. These can be due to (i) the intrinsic fiber coiling of single muscle types, or (ii) a difference in the tensional stress under which each muscle type is held in the organ.

To discriminate between these two possibilities, we next deduced the tensional stress of the T and L muscles in the whole-arm configuration by measuring the changes in dimensions of T and L muscle strips within the arm and upon dissection.

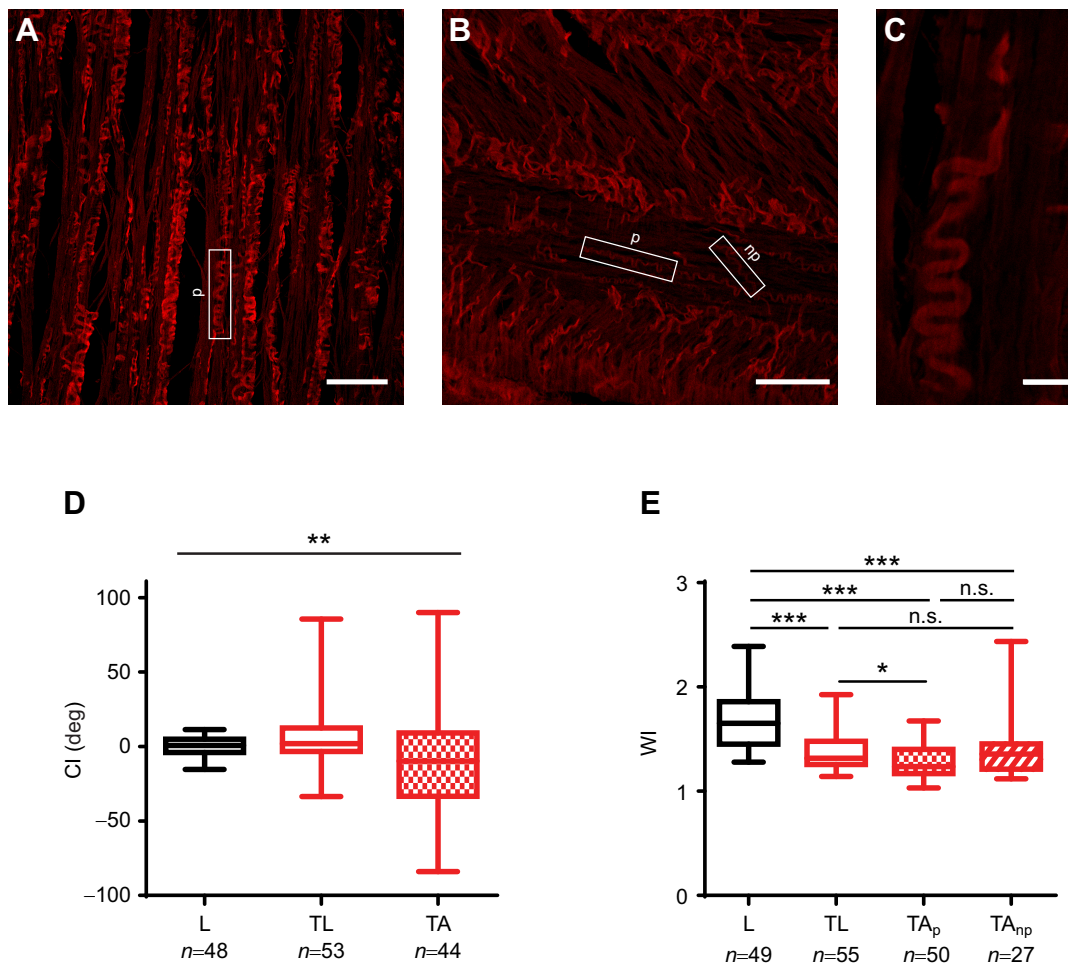


**Fig. 3. Elastic fiber organization.** (A–C) Confocal images of arm muscles stained with Picrosirius Red (PSR). Coiled elastic fibers (white rectangles) appear intensely red. (A) L muscles. Scale bar: 100  $\mu\text{m}$ . (B) T aboral muscles. Examples of parallel (p) and non-parallel (np) fibers are indicated by white rectangles. Scale bar: 100  $\mu\text{m}$ . (C) Detail of one L aboral coiled elastic fiber. Scale bar: 25  $\mu\text{m}$ . (D) CI for L, TL and TA (Kruskal–Wallis test,  $**P<0.01$ ). (E) WI for L, TL, parallel TA ( $TA_p$ ) and non-parallel TA ( $TA_{np}$ ) (Kruskal–Wallis test with Dunn’s multiple comparisons,  $*P<0.05$ ,  $**P<0.01$ ,  $***P<0.001$ ; n.s., not significant). Box plots show median (horizontal line inside boxes), upper and lower quartiles (box) and total range (whiskers).

### Muscle strain

In accordance with biomechanical experiments, the muscle resting length ( $L_R$ ) was considered to be that of the muscle strip once dissected from the arm. Measurements of T and L dimensions within the arm ( $L_{in}$ ) and upon dissection ( $L_R$ ) (from four different specimens) were compared, and  $L_{in}$  was expressed as a percentage of  $L_R$ . The results showed that the L and T muscles changed their dimensions upon dissection from the arm (Fig. 2B, L  $n=11$  samples, T  $n=10$  samples). In particular, in the whole-arm configuration, L muscles are compressed along their main force axis by about 20% of  $L_R$ , while T muscles are stretched by about 30% of their  $L_R$  (see dashed ellipses in Fig. 2B). These findings suggest that the observed difference in WI might depend on tensional stresses present in the whole-arm configuration.

To verify whether tensional stress can induce changes in muscle elastic fiber coiling, we next measured the WI for the T and L in whole-arm samples undergoing mechanical strain of 0%, 10% and 30% of the arm sample resting length.

As L muscle fibers are oriented along the longitudinal axis of the arm, when the whole arm is stretched, the L muscle undergoes the same mechanical strain that is applied to the whole arm, and all muscle elements (muscle fibers and connective tissue, including

elastic components) elongate. Conversely, T muscles, lying on planes perpendicular to the main axis of the arm, shorten. Given the arm cylindrical shape and the constant-volume constraint, all T muscle elements undergo a mechanical strain equal to the arm diameter’s reduction and proportional to the square root of the imposed length change. As expected, when whole-arm samples were stretched, coiled elastic fibers of the L muscles showed a significant decrease in WI (Fig. 4A; Kruskal–Wallis test with Dunn’s multiple comparisons test,  $P<0.01$  to  $P<0.001$ ), while those of the T muscles showed a significant increase (Fig. 4B; Kruskal–Wallis test with Dunn’s multiple comparisons test,  $P<0.001$ ).

These results show that mechanical stretching of the arm induces a modification in the intrinsic coiling of fibers. They also indirectly suggest that the strain imposed on the T and L muscles in the whole-arm configuration is a key determinant of their differences in WI in an arm at rest.

The coiling of the elastic fibers is a major component of soft tissue stress–strain properties that can be measured using parameters such as strain rate, sensitivity and hysteresis (Humphrey, 2003). We next performed a series of biomechanical tests to characterize T and L stress–strain properties, focusing particularly on stiffness and elastic hysteresis.

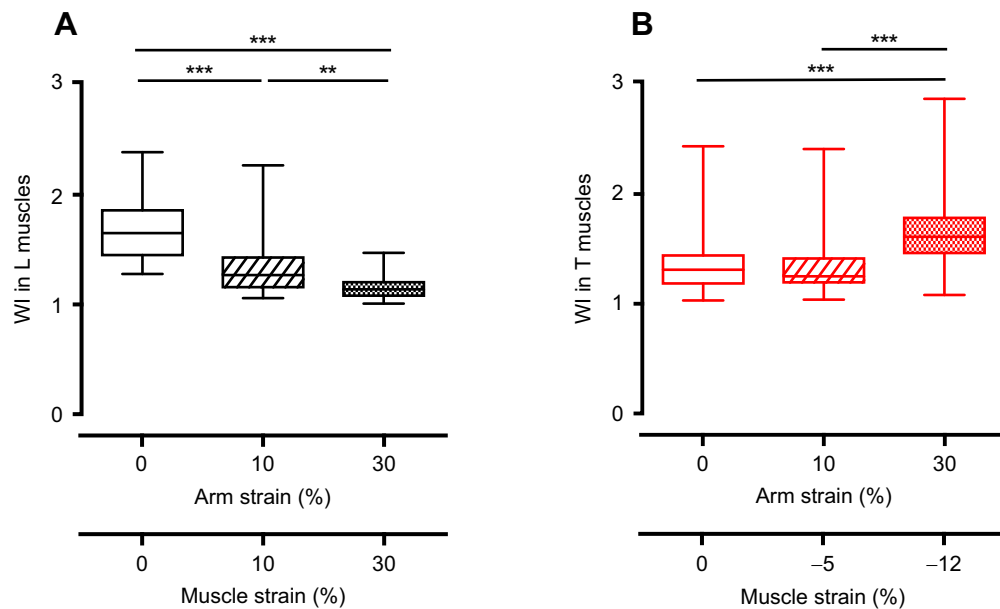


**Fig. 4. Waviness index.** WI of coiled elastic fibers in whole-arm samples undergoing a mechanical strain of 0%, 10% and 30% of the sample resting length. The imposed arm strain percentage and the resulting muscle strain percentage are reported on the x-axis. Given cylindrical shape of the arm, the constant-volume constraint and the muscle orientation along the arm, L muscles undergo the same mechanical strain imposed on the whole arm, and T muscles undergo a mechanical strain in the opposite direction proportional to the square root of the imposed strain (see Materials and Methods for details). (A) WI in L muscles. WI significantly decreased with arm elongation (Kruskal–Wallis test with Dunn’s multiple comparisons test, \*\* $P < 0.01$ , \*\*\* $P < 0.001$ ). (B) WI in T muscles. WI significantly increased with arm elongation (Kruskal–Wallis test with Dunn’s multiple comparisons test, \*\*\* $P < 0.001$ ).

### Stress–strain properties

Stress–strain properties are particularly relevant in hydrostatic muscles because they can strongly affect not only the force generated during movements, but also the ability to produce limb reconfiguration during motion. Here, we investigated the muscle stress–strain relationship, Young’s modulus and elastic hysteresis. To calculate the muscle stress–strain relationship and Young’s modulus, passive tension developed by the muscle under static strain conditions was measured with a stress–strain step-stretch protocol from 1% to 60% of the muscle  $L_R$  (Fig. S2; see Materials and Methods for details). Elastic hysteresis, representing the amount of energy dissipated during lengthening–shortening cycles, was investigated using a sinusoidal length-change protocol of  $\pm 30\%$   $L_R$  corresponding to half of the maximum length excursion used in the stress–strain protocol.

### Stress–strain relationship

Following the Hill model (Fig. S2), muscle response to mechanical strain is composed of an early peak force ( $F_{SE}$ ), mainly dependent upon SE elastic components, and a steady-state force ( $F_{PE}$ ), generated mainly by PE elastic components. The T and L stress–strain relationship and Young’s modulus were then deduced from these force components. The T muscles manifested significantly higher levels of stress ( $\sigma_{SE}$  and  $\sigma_{PE}$ ) compared with the L muscles starting from 45% to 50% of the strain (Fig. 5A,B; two-way RM-ANOVA with Šidák multiple comparisons,  $P < 0.05$  to  $P < 0.001$ ,  $n = 5$  for each experimental group).

Young’s modulus for the T muscles, calculated based on either the SE or PE components, was significantly higher than that manifested by the L muscles, respectively, from a high level of strain ( $E_{SE}$ , 45–60%) and from a medium–high level of strain ( $E_{PE}$ , 30–45%) (Fig. 5C,D; two-way RM-ANOVA with Šidák multiple comparisons,  $P < 0.05$  to  $P < 0.001$ ,  $n = 5$  for each experimental group).

These results suggest that T muscles are stiffer than L muscles. This finding might reflect the observed differences in the extracellular matrix and elastic fiber organization of the two muscles.

### Elastic hysteresis

Elastic hysteresis is typical of viscoelastic systems. Fully elastic systems tend to exhibit the same stress–strain curve during the elongation and shortening phases. Conversely, viscoelastic systems give rise to closed-loop stress–strain profiles where part of the energy injected into the system during the elongation phase is dissipated as heat due to material internal friction, thus resulting in a lower stress–strain curve during the shortening phase.

To investigate this property, we applied four cycles of  $\pm 30\%$   $L_R$  sinusoidal length changes to the muscle strips (12 L and 10 T) (Fig. 6A). The last two cycles were used to calculate the elastic hysteresis percentage as the ratio of energy dissipated ( $E_d$ ) to the total energy input ( $E_i$ ) to the system (Eqn 7). The L muscles showed a significantly higher hysteresis percentage than the T muscles, thus manifesting higher viscoelastic properties ( $t$ -test, Fig. 6B,  $P < 0.01$ ).

### DISCUSSION

Hydrostatic organs move by means of forces that are transmitted not through rigid skeletons but through internal pressure (Kier, 2012). In these structures, shape deformations occur through the passive and active control of dimensional changes involving the concomitant action of connective tissue and muscular elements. The muscle’s ability to produce passive tension is influenced by several factors, including the presence of intramuscular titin protein, intramuscular connective tissues (Huijing, 1999; Schleip et al., 2006) and even intracellular fluid (Kier, 2020; Sleboda and Roberts, 2017). Connective tissue makes up the muscle’s extracellular matrix and, in muscular hydrostats, plays a critical

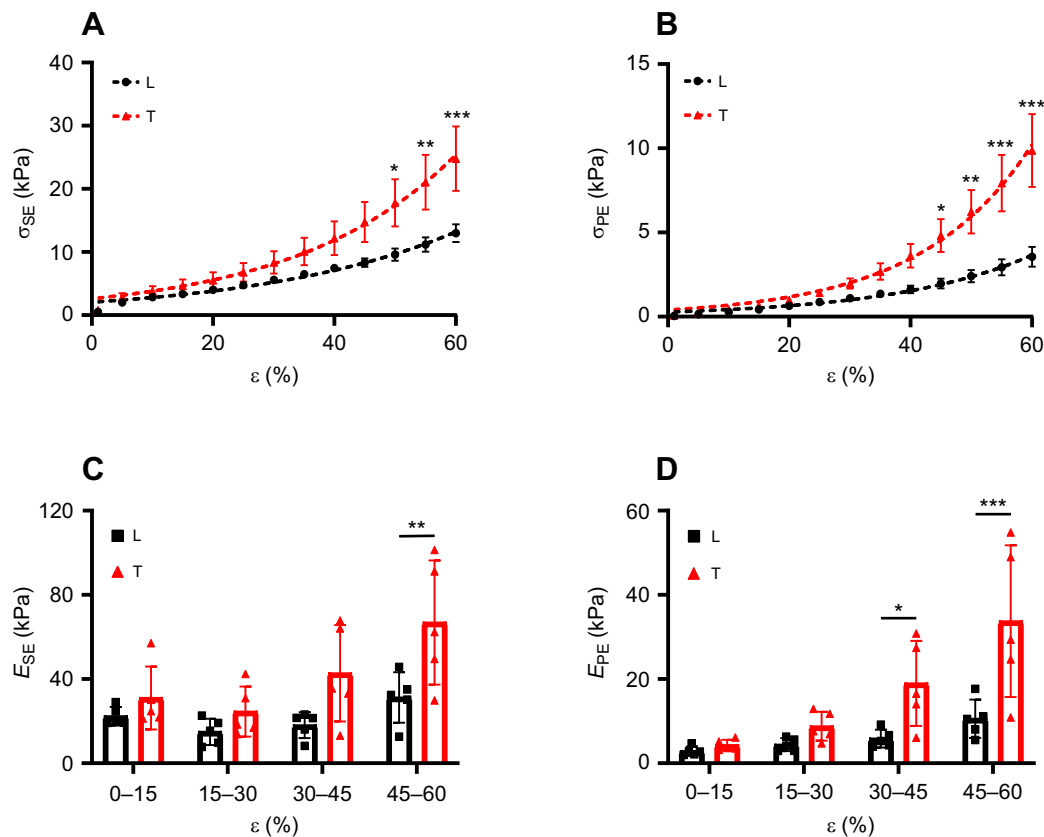


**Fig. 5. Muscle stress-strain relationship.** (A) L and T muscle stress–strain relationship of the series elastic (SE) component (means $\pm$ s.e.m.). T muscles manifested a significantly higher level of stress ( $\sigma_{SE}$ ) from 50% of strain ( $\epsilon$ ) (two-way RM-ANOVA with Šidák multiple comparisons, \* $P$ <0.05, \*\* $P$ <0.01, \*\*\* $P$ <0.001,  $n$ =5 for each experimental group). (B) L and T stress–strain relationship of the parallel elastic (PE) component (means $\pm$ s.e.m.). T muscles manifested a significantly higher level of stress ( $\sigma_{PE}$ ) from 45% of strain (two-way RM-ANOVA with Šidák's multiple comparisons test, \* $P$ <0.05, \*\* $P$ <0.01, \*\*\* $P$ <0.001,  $n$ =5 for both experimental groups). (C) Young's modulus for L and T muscles, calculated based on SE components ( $E_{SE}$ ). T muscle  $E_{SE}$  was significantly higher than L muscle  $E_{SE}$  from a high level of strain (45–60%) (two-way RM-ANOVA with Šidák's multiple comparisons test, \*\* $P$ <0.01,  $n$ =5 for both experimental groups, symbols are individual data points, bars show means and s.d.). (D) Young's modulus for L and T muscles calculated based on PE components ( $E_{PE}$ ). T muscle  $E_{PE}$  was significantly higher than L muscle  $E_{PE}$  at medium–high (30–45%) and high (45–60%) levels of strain (two-way RM-ANOVA with Šidák's multiple comparisons test, \* $P$ <0.05, \*\*\* $P$ <0.001,  $n$ =5 for both experimental groups, symbols are individual data points, bars show means and s.d.).

role in controlling shape and motions, as it can provide structural reinforcement during muscle stiffening, transmit stress and store elastic energy. Recent studies have reported that forces transmitted

by hydrostatic pressure in the muscle to the fibers of the extracellular matrix affect muscle strain and significantly contribute to muscle mechanics in both their active contraction and passive elongation

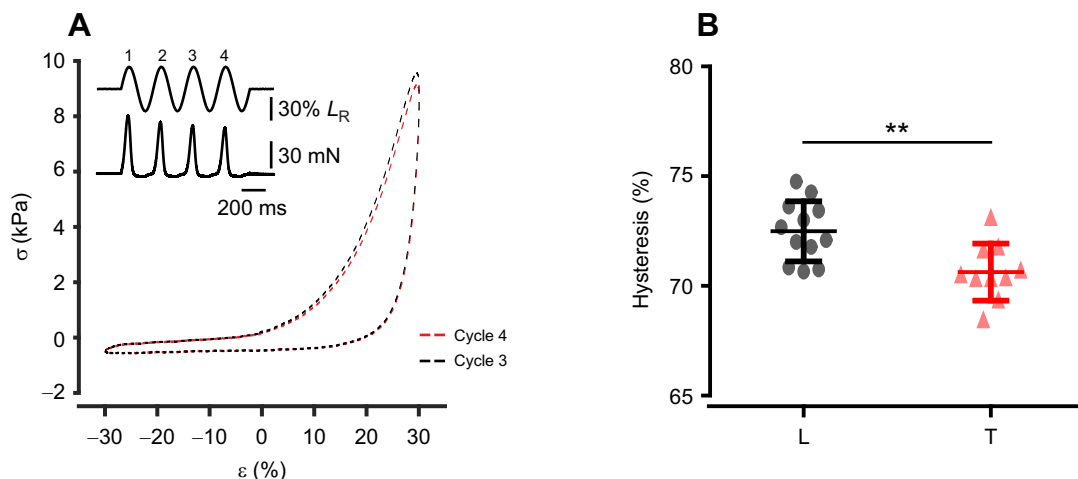


**Fig. 6. Hysteresis loop.** (A) Exemplary force–position traces and corresponding hysteresis loops obtained from the third and fourth cyclic sinusoidal length change. (B) Hysteresis percentage for L ( $n$ =12) and T ( $n$ =10) (means $\pm$ s.d.). L muscles showed a significantly higher hysteresis percentage ( $t$ -test, \*\* $P$ <0.01).

(Sleboda and Roberts, 2020). Moreover, it is well known that animals exploit the elastic properties of their muscles in different ways. As an example, elastic components can influence the speed of the contractile elements, allowing muscles to attain higher performance levels, inducing metabolic energy savings during various modes of locomotion, and affecting the force–position control of muscles (Alexander, 2002).

Muscles in hydrostatic structures can also be subject to different levels of pressure, depending on their position and function within the animal body. This aspect is extremely important, as it allows unconstrained muscles to quickly and efficiently adapt to large-length excursion and to modulate their biomechanical response in a length-dependent manner (Kier, 2020; Sleboda and Roberts, 2017, 2020).

Here, we show that internal hydrostatic pressures are inherently present within the octopus arm, and they have a distinct effect on the strain of the T and L arm muscles, thus determining the different coiling rates of the muscle elastic fiber components (see Fig. 2B). Notably, owing to the intrinsic relationship between arm diameter and length, each muscle rate of coiling is in line with its need to accommodate either a higher (for L muscles) or a lower (for T muscles) magnitude of deformation occurring during arm lengthening. A similar finding was obtained by a study on the squid body wall muscular hydrostat, demonstrating the presence of a particular type of ‘helically wound intramuscular collagen fibers’, inducing a non-uniform strain across the muscular body and altered by the increase or decrease in lateral compression occurring during respiratory actions (Kurth et al., 2014).

Other than tensional stress, we found that arm muscles also have an intrinsic difference in their viscoelasticity, with T muscles showing a significantly higher stiffness than L muscles (Fig. 5A,B). This additionally influences passive muscle responses to changes in tensional stress that occur during motion.

One tempting possibility is that the observed difference is driven, at least partially, by the organization of the elastic fibers in the extracellular matrix arranged along the main muscle force vector in the L muscles and more chaotically in the T muscles. This matrix organization is functional in several arm deformations and may allow for a reduction in energy consumption during motion.

For instance, during arm elongation, L muscles undergo a significant variation in length that might be facilitated by the passive uncoiling of the L compressed elastic fibers (increasing the arm length) along with the recoiling of the T elongated elastic fibers (reducing the arm CSA). Likewise, during arm bending, L muscles shorten by active contraction of muscle fibers on the bending side and concomitant passive uncoiling of L elastic elements on the opposite side of the arm, while the higher stiffness of T muscles allows the arm to resist a diameter increase (a condition necessary to produce bending).

T muscle passive stiffness also has an important role in supporting a variety of motions, such as walking and fetching; this is in line with T muscles’ active biomechanical properties, suggesting their involvement in posture maintenance and load-bearing functions.

It has been shown that most arm deformations occur within the first two-thirds of the arm length (Huffard et al., 2005; Kennedy et al., 2020; Levy et al., 2015) where the T muscles are mostly represented. Hence, in the octopus arm, differences in muscle elasticity and stiffness might be used to specify their role during movement and to allow for a reduction in the energetic cost of motion; this happens in a variety of organs of different animals (Gosline et al., 1983; Lillie and Gosline, 2006). In the circumstances described above, elastic elements can thus act as intramuscular

locomotor springs, allowing muscle power amplification (through elasticity) or power attenuation (through stiffening) and thus affecting the dynamics of movement resulting from muscle activity.

The potential contribution of muscle springs to locomotion should also be considered in the context of natural motions. Muscles are often involved in rhythmic activities such as running, swimming and breathing, where they undergo cyclic lengthening and shortening. In these cases, the elastic energy affecting motions will depend on the amount of energy the spring can store and return to the system (Full and Meijer, 2004). This feature is identified as ‘hysteresis’ and expresses the rate of energy dissipated due to internal friction during cyclic shortening/lengthening. Here, we show that L muscles have a higher hysteresis percentage than T muscles, which is indicative of a higher viscoelasticity of the L layers of the arm muscle bulk. This difference suggests that longitudinal arm muscles might play a role as shock absorbers through the dissipation, as heat, of a substantial part of the energy incorporated during lengthening, a property known as ‘damping’. Damping retains enormous relevance in the context of motor control, as it can reduce oscillation in motion, decrease the need for corrective neural control (Franklin et al., 2004) and, in general, increase motion stability. Damping is especially relevant for aquatic animals that must cope with fluid dynamic forces that can be unsteady and turbulent, and that might affect motion execution.

Moreover, the elastic passive elements might react more rapidly than the speed at which the nervous system can process, thus making the classical feedback mechanism of motion control and correction unnecessary (Tytell et al., 2018). Hence, octopus body mechanics and their tissue components represent an embodied solution that reacts autonomously and rapidly to environmental perturbations.

Taken together, we suggest that connective tissue elasticity and passive stiffness of the arm muscles have developed, together with their activation properties, to fit their role in arm use. Moreover, the organization of elastic elements allows muscles to operate beyond their intrinsic contractile properties and brings a global reduction to the energetic and computational cost of arm motion. This aspect is also particularly relevant within the field of soft-robotics, as an increasing number of researchers are currently aiming at designing and constructing bio-inspired soft-robotic manipulators capable of semi-autonomous functions (Kang et al., 2016; Kier, 2012; Laschi et al., 2009; Nakajima et al., 2018; Xu et al., 2019; Zullo et al., 2012). However, many bottlenecks limit the full translation of biology into robotics. We believe that these studies may make an important contribution to the field, allowing for the implementation of morphological and passive biomechanical determinants of arm performance.

## Conclusion

In this work, we showed the presence of intrinsic tensional stresses in the octopus arm, affecting both muscle strain and the coiling of intramuscular elastic fibers. This configuration might have developed to cope with changes in arm strain that inevitably occur during motion. The structure and arrangement of the extracellular matrix configuration within each muscle type supports the role of the longitudinal muscles in energy storage and release, allowing energy saving and stabilization of motion (possibly through a damping effect) and that of the transverse musculature in resistance to passive deformation and posture maintenance. The elastic fiber configuration of the octopus arm therefore underpins the specific role of each muscle during movement and may contribute to several aspects of the arm locomotor performance, from mechanics to energetic and neural control.



**Acknowledgements**

We thank Benny Hochner for valuable discussions and the animal facility for animal care and maintenance.

**Competing interests**

The authors declare no competing or financial interests.

**Author contributions**

Conceptualization: L.Z.; Methodology: A.D.C., F.M.; Validation: A.D.C., L.Z.; Formal analysis: A.D.C., F.M.; Investigation: A.D.C., F.M., I.B.; Resources: L.Z.; Data curation: A.D.C., F.M., I.B.; Writing - original draft: L.Z., A.D.C.; Writing - review & editing: L.Z., A.D.C.; Visualization: I.B.; Supervision: L.Z.; Project administration: L.Z.; Funding acquisition: L.Z.

**Funding**

This work was supported by the Seventh Framework Programme (OCTOPUS IP, Project Number FP7-231608), by the European Cooperation in Science and Technology (FA 1301 CephInAction) and by the Office of Naval Research (award number N00014-21-1-2516).

**References**

- Alexander, R. M.** (2002). Tendon elasticity and muscle function. *Comp. Biochem. Physiol. A Mol. Integr. Physiol.* **133**, 1001-1011. doi:10.1016/S1095-6433(02)00143-5
- Baxi, J., Barclay, C. J. and Gibbs, C. L.** (2000). Energetics of rat papillary muscle during contractions with sinusoidal length changes. *Am. J. Physiol. Heart Circ. Physiol.* **278**, H1545-H1554. doi:10.1152/ajpheart.2000.278.5.H1545
- Fiorito, G., Affuso, A., Anderson, D. B., Basil, J., Bonnaud, L., Botta, G., Cole, A., D'Angelo, L., De Girolamo, P., Dennison, N. et al.** (2014). Cephalopods in neuroscience: regulations, research and the 3Rs. *Invert. Neurosci.* **14**, 13-36. doi:10.1007/s10158-013-0165-x
- Fiorito, G., Affuso, A., Basil, J., Cole, A., de Girolamo, P., D'angelo, L., Dickel, L., Gestal, C., Grasso, F., Kuba, M. et al.** (2015). Guidelines for the care and welfare of cephalopods in research—A consensus based on an initiative by CephRes, FELASA and the boyd group. *Lab. Anim.* **49**, 1-90. doi:10.1177/0023677215580006
- Fossati, S. M., Benfenati, F. and Zullo, L.** (2011). Morphological characterization of the *Octopus vulgaris* arm. *Vie Milieu* **61**, 197-201.
- Franklin, D. W., So, U., Kawato, M. and Milner, T. E.** (2004). Impedance control balances stability with metabolically costly muscle activation. *J. Neurophysiol.* **92**, 3097-3105. doi:10.1152/jn.00364.2004
- Full, R. and Meijer, K.** (2004). Metrics of natural muscle function. In *Electroactive Polymer (EAP) Actuators as Artificial Muscles: Reality, Potential, and Challenges*, chapter 3 (ed. Y. Bar-Cohen). SPIE Press.
- Gosline, J. M., Steeves, J. D., Harman, A. D. and Demont, M. E.** (1983). Patterns of circular and radial mantle muscle activity in respiration and jetting of the squid *Loligo opalescens*. *J. Exp. Biol.* **104**, 97. doi:10.1242/jeb.104.1.97
- Graziadei, P.** (1971). The nervous system of the arms. In *The Anatomy of the Nervous System of Octopus vulgaris* (ed. J. Z. Young), pp. 45-62. Oxford: Oxford University Press.
- Hill, A. V.** (1938). The heat of shortening and the dynamic constants of muscle. *Proc. R. Soc. B Biol. Sci.* **126**, 136-195. doi:10.1098/rspb.1938.0050
- Huffard, C. L., Boneka, F. and Full, R. J.** (2005). Underwater bipedal locomotion by octopuses in disguise. *Science* **307**, 1927. doi:10.1126/science.1109616
- Huijijng, P. A.** (1999). Muscle as a collagen fiber reinforced composite: a review of force transmission in muscle and whole limb. *J. Biomech.* **32**, 329-345. doi:10.1016/S0021-9290(98)00186-9
- Humphrey, J.** (2003). Continuum biomechanics of soft biological tissues. *Proc. R. Soc. A Math. Phys. Eng. Sci.* **459**, 3-46. doi:10.1098/rspa.2002.1060
- Josephson, R. K.** (1985). Mechanical power output from striated muscle during cyclic contraction. *J. Exp. Biol.* **114**, 493-512. doi:10.1242/jeb.114.1.493
- Kang, R., Guglielmino, E., Zullo, L., Branson, D. T., Godage, I. and Caldwell, D. G.** (2016). Embodiment design of soft continuum robots. *Adv. Mech. Eng.* **8**, 1-13. doi:10.1177/1687814016643302
- Kennedy, E. B. L., Buresch, K. C., Boinapally, P. and Hanlon, R. T.** (2020). Octopus arms exhibit exceptional flexibility. *Sci. Rep.* **10**, 20872. doi:10.1038/s41598-020-77873-7
- Kier, W. M.** (2012). The diversity of hydrostatic skeletons. *J. Exp. Biol.* **215**, 1247-1257. doi:10.1242/jeb.056549
- Kier, W. M.** (2016). The musculature of coleoid cephalopod arms and tentacles. *Front. Cell Dev. Biol.* **4**, 10. doi:10.3389/fcell.2016.00010
- Kier, W. M.** (2020). Muscle force is modulated by internal pressure. *Proc. Natl. Acad. Sci. USA* **117**, 2245-2247. doi:10.1073/pnas.1921726117
- Kier, W. M. and Stella, M. P.** (2007). The arrangement and function of octopus arm musculature and connective tissue. *J. Morphol.* **268**, 831-843. doi:10.1002/jmor.10548
- Kurth, J. A., Thompson, J. T. and Kier, W. M.** (2014). Connective tissue in squid mantle is arranged to accommodate strain gradients. *Biol. Bull.* **227**, 1-6. doi:10.1086/BBLv227n1p1
- Laschi, C., Mazzolai, B., Mattoli, V., Cianchetti, M. and Dario, P.** (2009). Design of a biomimetic robotic octopus arm. *Bioinspir. Biomim.* **4**, 015006. doi:10.1088/1748-3182/4/1/015006
- Levy, G., Flash, T. and Hochner, B.** (2015). Arm coordination in octopus crawling involves unique motor control strategies. *Curr. Biol.* **25**, 1195-1200. doi:10.1016/j.cub.2015.02.064
- Lillie, M. A. and Gosline, J. M.** (2006). Tensile residual strains on the elastic lamellae along the porcine thoracic aorta. *J. Vasc. Res.* **43**, 587-601. doi:10.1159/000096112
- Nakajima, R., Shigeno, S., Zullo, L., De Sio, F. and Schmidt, M. R.** (2018). Cephalopods between Science, Art, and Engineering: A Contemporary Synthesis. *Frontiers in Communication*, **3**, art. no. 20. doi:10.3389/fcomm.2018.00020
- Schleip, R., Naylor, I. L., Ursu, D., Melzer, W., Zorn, A., Wilke, H.-J., Lehmann-Horn, F. and Klingler, W.** (2006). Passive muscle stiffness may be influenced by active contractility of intramuscular connective tissue. *Med. Hypotheses* **66**, 66-71. doi:10.1016/j.mehy.2005.08.025
- Sleboda, D. A. and Roberts, T. J.** (2017). Incompressible fluid plays a mechanical role in the development of passive muscle tension. *Biol. Lett.* **13**, 20160630. doi:10.1098/rsbl.2016.0630
- Sleboda, D. A. and Roberts, T. J.** (2020). Internal fluid pressure influences muscle contractile force. *Proc. Natl. Acad. Sci. USA* **117**, 1772-1778. doi:10.1073/pnas.1914433117
- Syme, D. A. and Stevens, E. D.** (1989). Effect of cycle frequency and excursion amplitude on work done by rat diaphragm muscle. *Can. J. Physiol. Pharmacol.* **67**, 1294-1299. doi:10.1139/y89-206
- Thompson, J. T. and Kier, W. M.** (2001). Ontogenetic changes in fibrous connective tissue organization in the oval squid, *Sepioteuthis lessoniana* Lesson, 1830. *Biol. Bull.* **201**, 136-153. doi:10.2307/1543329
- Tytell, E. D., Carr, J. A., Danos, N., Wagenbach, C., Sullivan, C. M., Kiemel, T., Cowan, N. J. and Ankarali, M. M.** (2018). Body stiffness and damping depend sensitively on the timing of muscle activation in lampreys. *Integr. Comp. Biol.* **58**, 860-873. doi:10.1093/icb/icy042
- Vogel, B., Siebert, H., Hofmann, U. and Frantz, S.** (2015). Determination of collagen content within picrosirius red stained paraffin-embedded tissue sections using fluorescence microscopy. *MethodsX* **2**, 124-134. doi:10.1016/j.mex.2015.02.007
- Xu, P. A., Mishra, A. K., Bai, H., Aubin, C. A., Zullo, L. and Shepherd, R. F.** (2019). Optical lace for synthetic afferent neural networks. *Sci. Robot.* **4**, eaaw6304. doi:10.1126/scirobotics.aaw6304
- Zullo, L., Fossati, S. M. and Benfenati, F.** (2011). Transmission of sensory responses in the peripheral nervous system of the arm of *Octopus vulgaris*. *Vie Milieu* **61**, 197-201.
- Zullo, L., Chiappalone, M., Martinoia, S. and Benfenati, F.** (2012). A "spike-based" grammar underlies directional modification in network connectivity: effect on bursting activity and implications for bio-hybrids systems. *PLoS ONE* **7**, e49299. doi:10.1371/journal.pone.0049299
- Zullo, L., Eichenstein, H., Maiolo, F. and Hochner, B.** (2019). Motor control pathways in the nervous system of *Octopus vulgaris* arm. *J. Comp. Physiol. A* **205**, 271-279. doi:10.1007/s00359-019-01332-6

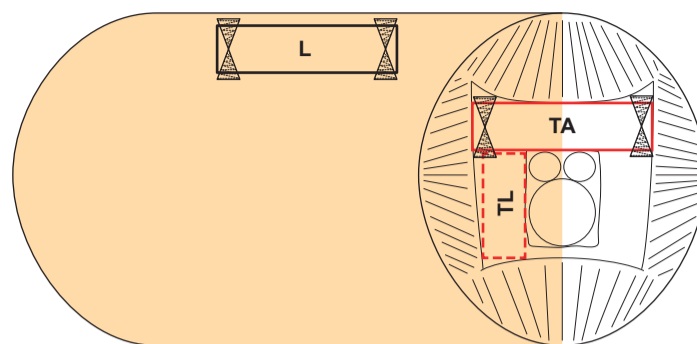


**Fig. S1. Arm muscle dissection methodology employed for biomechanics and histology.** Transverse aboral (TA, red box), transverse lateral (TL, dashed red box), longitudinal muscle (L, black box) and the position of the knots used to tighten the muscle strips to the Dual Mode Lever arm system are represented.

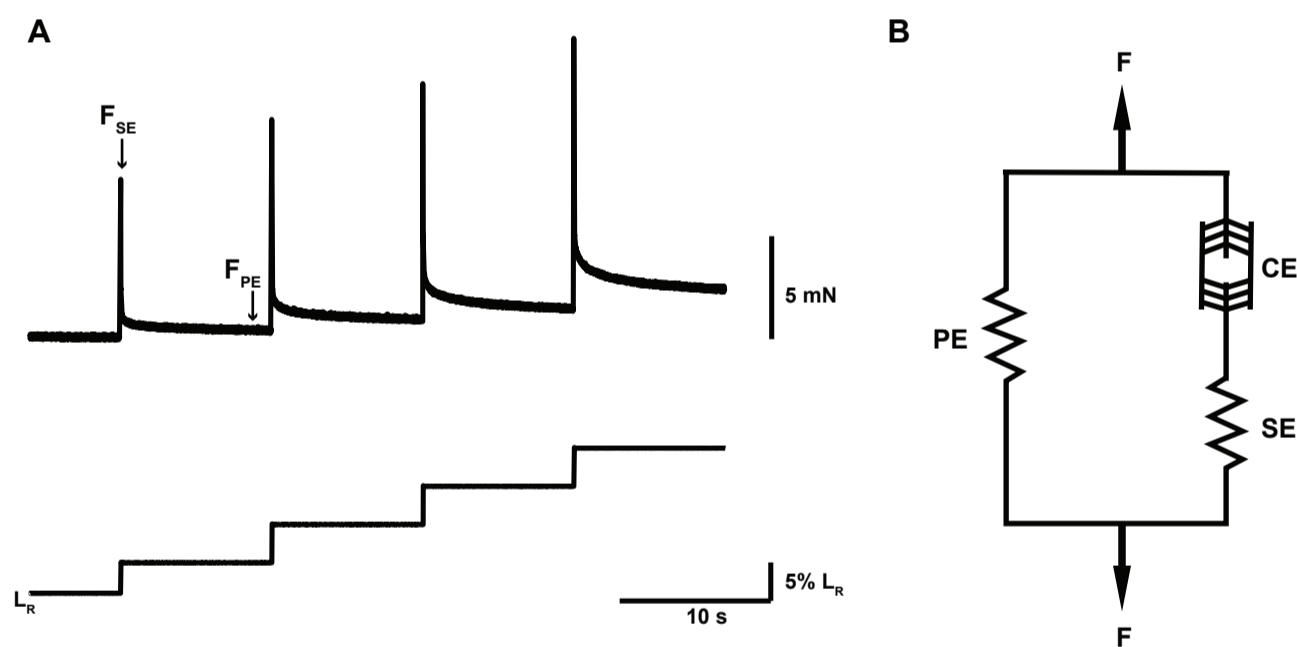


**Fig. S2. Elastic and contractile elements of muscle forces.** (A) Representative traces of the step-stretch protocol. The positions along the traces where the SE elastic force ( $F_{SE}$ ) and the PE elastic force ( $F_{PE}$ ) were measured are indicated by the arrows. (B) Hill model/diagram showing contractile component (CE), parallel elastic component (PE), series elastic component (SE) and the resulting force (F).

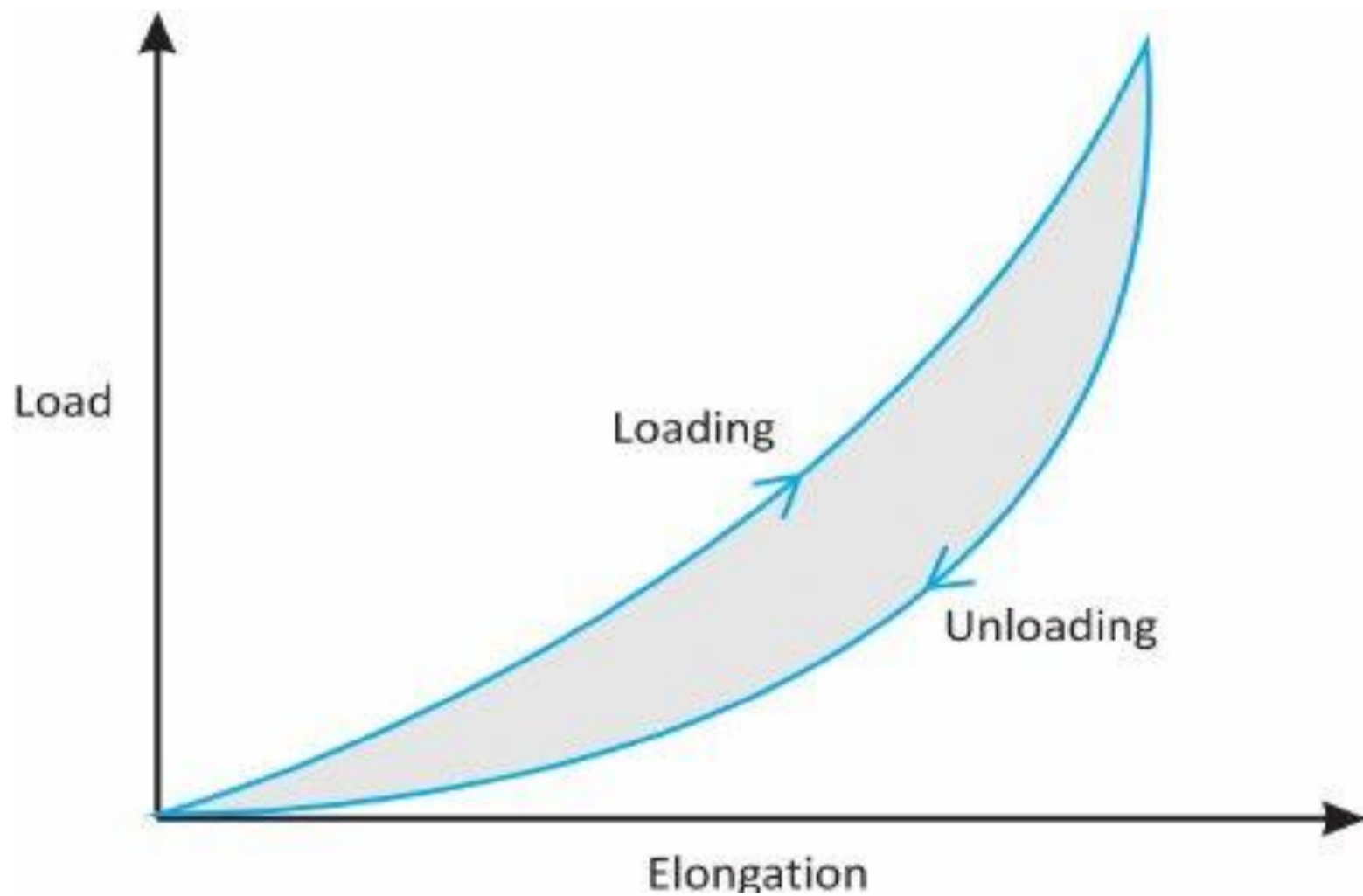


**Fig. S3. Hysteresis percentage.** Stress-strain curves during the loading and unloading phases (blue lines). Total energy input to the system is calculated as the area under the loading phase ( $E_i$ , red lines in the graph). The energy dissipated is represented by the area enclosed between the loading and unloading phases ( $E_d$ , gray area in the graph) and is calculated as the difference between the area under the loading phase and the area under the unloading phase.